Optical Engineering

SPIEDigitalLibrary.org/oe

Total integrated scatter from surfaces with arbitrary roughness, correlation widths, and incident angles

James E. Harvey
Sven Schröder
Narak Choi
Angela Duparré

Total integrated scatter from surfaces with arbitrary roughness, correlation widths, and incident angles

James E. Harvey
The University of Central Florida
The Center for Research and Education in Optics and Lasers (CREOL)
P.O. Box 162700, 4000 Central Florida Blvd.
Orlando, Florida 32826
E-mail: harvey@creol.ucf.edu

Sven Schröder
Fraunhofer Institute for Applied Optics and Precision Engineering
Albert-Einstein-Straße 7
07745 Jena, Germany

Narak Choi
The University of Central Florida
The Center for Research and Education in Optics and Lasers (CREOL)
P.O. Box 162700, 4000 Central Florida Blvd.
Orlando, Florida 32826

Angela Duparré
Fraunhofer Institute for Applied Optics and Precision Engineering
Albert-Einstein-Straße 7
07745 Jena, Germany

Abstract. Surface scatter effects from residual optical fabrication errors can severely degrade optical performance. The total integrated scatter (TIS) from a given mirror surface is determined by the ratio of the spatial frequency band-limited "relevant" root-mean-square surface roughness to the wavelength of light. For short-wavelength (extreme-ultraviolet/x-ray) applications, even state-of-the-art optical surfaces can scatter a significant fraction of the total reflected light. In this paper we first discuss how to calculate the band-limited relevant roughness from surface metrology data, then present parametric plots of the TIS for optical surfaces with arbitrary roughness, surface correlation widths, and incident angles. Surfaces with both Gaussian and *ABC* or *K*-correlation power spectral density functions have been modeled. These parametric TIS predictions provide insight that is useful in determining realistic optical fabrication tolerances necessary to satisfy specific optical performance requirements.
 [DOI: 10.1117/1.OE.51.1.013402]

Subject terms: surface scatter; total integrated scatter; TIS; scattering from rough surfaces; bidirectional reflectance distribution function; BRDF; surface power spectral density function; PSD; relevant band-limited roughness.

Paper 110928 received Aug. 3, 2011; revised manuscript received Oct. 18, 2011; accepted for publication Nov. 17, 2011; published online Feb. 6, 2012.

1 Introduction and Overview

Surface scatter phenomena continue to be an important issue in diverse areas of science and engineering in the 21st century. In some applications, the total amount of scattered radiation is of primary concern. In other applications, knowing the angular distribution of the scattered light is crucial.

Recall that the reflectance of a surface is defined as the ratio of the (total) reflected radiant power divided by the incident radiant power. However, for real surfaces (exhibiting some residual surface roughness) the total reflected radiant power consists of two components: one specularly reflected (obeying the law of reflection) and the other diffusely reflected (scattered).

Following the work of Bennett and Porteus,[1] which built upon the earlier work of Davies,[2] the fraction of the total reflected radiant power remaining in the specular beam after reflection from a single moderately rough surface is given by

$$\frac{R_s}{R_t} = \exp[-(4\pi \cos\theta_i \sigma/\lambda)^2], \tag{1}$$

where R_s is the specular reflectance, R_t is the total reflectance, θ_i is the incident angle, σ is the root-mean-square (rms) surface roughness, and λ is the wavelength of the incident radiation.

The classical definition of total integrated scatter (TIS) follows directly from Eq. (1) as that fraction of the total reflected radiant power that is scattered out of the specularly reflected beam:

$$\begin{aligned} TIS &= \frac{\text{diffuse reflectance}}{\text{total reflectance}} \\ &= \frac{\text{diffuse reflectance}}{\text{specular reflectance} + \text{diffuse reflectance}} \\ &= \frac{R_d}{R_s + R_d}, \end{aligned} \tag{2}$$

or, since $R_d = R_t - R_s$, we obtain

$$TIS = \frac{R_t - R_s}{R_t} = 1 - \frac{R_s}{R_t} = 1 - \exp[-(4\pi \cos\theta_i \sigma/\lambda)^2]. \tag{3}$$

The above definition of TIS and its paraxial smooth surface approximation (for normal incidence)

$$TIS \approx (4\pi\sigma/\lambda)^2 \tag{4}$$

have been discussed extensively in the literature.[3–12] Unfortunately, the widely used commercially available ASAP

0091-3286/2012/$25.00 © 2012 SPIE

(Advanced Systems Analysis Program) optical analysis code defines the quantity TIS to be identical with the definition of diffuse reflectance.[13] Hence, the above definition of TIS is not always applied uniformly and consistently in the literature, in spite of the fact that there have been international standard procedures written for the measurement of TIS as a means of determining the roughness of a surface.[14]

An international standard has also been established defining total scattering (TS) as the ratio of the diffusely scattered radiant power to the incident radiant power.[15] TS directly expresses the scattered radiant power regardless of the reflectance of the surface. Although using TS has several advantages in practical integrated scatter measurements with respect to robustness and comparability among different metrology instruments, we use TIS in this paper for historical reasons and because all theoretical expressions are independent of R_t. The relationship between the two quantities is given simply by $\mathrm{TS} = \mathrm{TIS}\, R_t$.

After repeated discussions and admonitions by Church,[6,16] Church and Takacs,[17,18] Stover,[19] Germer and Asmail,[20] Dittman,[21,22] and others, most of the optical surface metrology community is aware that when we associate surface roughness with scattered light, we must specify the spatial frequency band limits of the effective roughness that is relevant to the particular scattering application. In other words, we must replace the total or intrinsic rms roughness, σ, with the *relevant* band-limited rms roughness, σ_{rel}, in Eqs. (3) and (4); hence TIS is

$$TIS = 1 - \exp[-(4\pi \cos\theta_i\, \sigma_{\mathrm{rel}}/\lambda)^2], \tag{5}$$

which for smooth surfaces can be approximated as

$$TIS \approx (4\pi \cos\theta_i\, \sigma_{\mathrm{rel}}/\lambda)^2 \tag{6}$$

In the remainder of this paper we will first discuss the statistical surface characteristics relevant to the scattering process and illustrate precisely how to calculate σ_{rel} for arbitrary surface power spectral density (PSD) functions, incident angles, and wavelengths. We will then provide parametric plots of $\sigma^2_{\mathrm{rel}}/\sigma^2_{\mathrm{total}}$ for optical surfaces as functions of surface correlation width for both Gaussian and *ABC* or *K*-correlation PSD functions.

We will then use Eq. (5) to make parametric TIS predictions that provide useful insight for determining realistic optical fabrication tolerances necessary to satisfy specific optical performance requirements. Finally, we will briefly demonstrate the capabilities of the generalized Harvey-Shack surface scatter theory in producing *angle resolved scatter* (ARS) or *bidirectional reflectance distribution function* (BRDF) curves for optical surfaces with arbitrary surface roughness (up to at least a few waves, an actual limit has not been established), correlation widths, and incident angles.

2 Surface Characteristics

The behavior of light scattered from randomly rough surfaces is dictated by the statistical surface characteristics. Consider the surface profile illustrated in Fig. 1. The surface has a zero mean with the surface height, h, illustrated as a function of position along a one-dimensional trace of finite length. Two relevant statistical surface characteristics are the surface height distribution function and the surface autocovariance (ACV) function.[9] Fortunately, for many cases of interest, the surface heights are normally distributed (i.e., the surface height distribution function is Gaussian). The rms surface roughness, σ_s, is the standard deviation of that normal distribution.

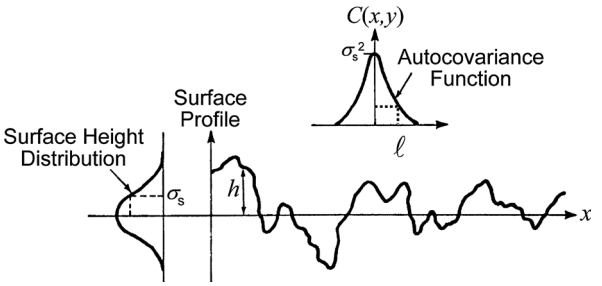

Fig. 1 Schematic diagram of a surface profile and its relevant statistical parameters.

Although it would be convenient (mathematically) if the surface ACV function were also Gaussian, in most instances that is not the case. Instead, the ACV function is material and process dependent. The ACV length, ℓ, is usually defined as the half-width of the ACV function at the $1/e$ height.

The surface PSD function and the surface ACV function are Fourier transforms of each other. Note in Fig. 1 that the value of the surface ACV function at the origin is equal to the surface variance, σ_s^2. From the central ordinate theorem of Fourier transform theory, we therefore know that the volume under the $2-D$ surface PSD is also equal to the surface variance.

The surface PSD can be thought of as a plot of surface variance as a function of the spatial frequency of the surface irregularities. We can thus talk about several different spatial frequency regimes that have distinctly different effects upon image quality, as illustrated in Fig. 2.

After decades of concerning themselves with only low spatial frequency "figure" errors and high spatial frequency "finish" errors or "microroughness," optical manufacturers are finally realizing the significance of "midspatial frequency" optical surface irregularities in the degradation of image quality.[23–25]

The low spatial frequency figure-error regime gives rise to conventional wavefront aberrations. The high spatial frequency finish-error/microroughness regime produces wideangle scattering effects that redistribute radiant energy from the image core into a broad scattered halo without substantially affecting the width of the image core. And the midspatial frequency regime that spans the gap between the traditional figure and finish errors produces small angle scatter that broadens or smears out the image core.[26–28]

Historically, optical fabrication tolerances have been specified by placing a tolerance upon only the figure and finish errors. It has only recently become common practice to also specify and measure the midspatial frequency surface irregularities.

The astronomer's classical definition of resolution has been the full width at half-max (FWHM) of the point spread function. For bright point sources, this image quality criterion is quite insensitive to wide-angle scatter resulting from high spatial frequency microroughness, since the width of the image core is not significantly broadened. However, for faint point sources, the wide-angle scattered halo causes

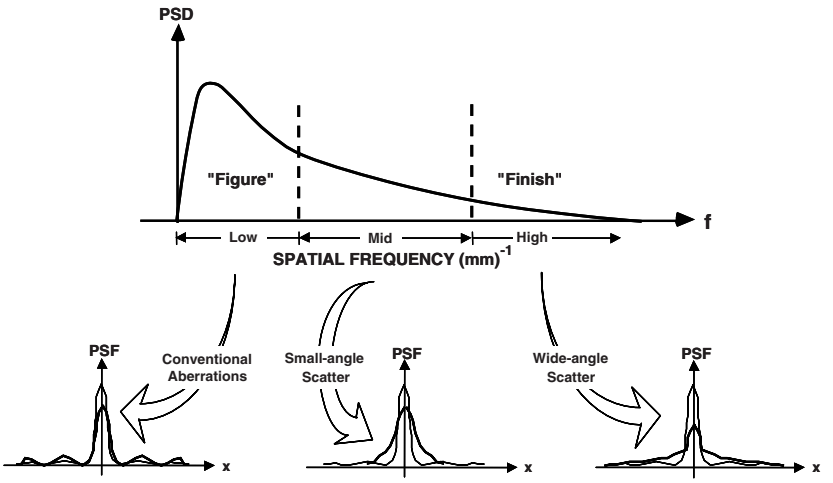

Fig. 2 Different spatial frequency regimes and their resulting effects upon image quality.

severe signal-to-noise problems and a substantial loss of image contrast. The small-angle scatter produced by the midspatial frequency surface irregularities does broaden the image core and therefore causes a significant decrease in resolution (larger FWHM). The same considerations hold for deep ultraviolet and especially for extreme ultraviolet (EUV) lithography applications.[29–32] It is thus imperative that optical fabrication tolerances be specified over the entire range of relevant spatial frequencies.

A uniformly rough surface is one whose roughness is homogeneous and isotropic, i.e., the surface height distribution function and the ACV function do not change with location or orientation of the (finite) measured surface profile. For such a surface, the PSD is a $2-D$ rotationally symmetric function.

It is important to recognize that the *relevant* (or effective) surface roughness is not an intrinsic surface characteristic, but a band-limited quantity that depends upon the wavelength and incident angle.[16,18] For normal incidence, those spatial frequencies greater than $1/\lambda$ produce evanescent (imaginary) waves that do not result in radiant power being scattered from the specular beam—i.e., spatial frequencies greater than $1/\lambda$ are completely irrelevant with regard to scattered light.[6] For an arbitrary incident angle, θ_i, the $2-D$ boundary of the appropriate bandlimited portion of the surface PSD is illustrated in Fig. 3(a), i.e., a circle of radius $1/\lambda$ whose center is shifted to a spatial frequency[33] given by

$$f_o = \frac{\sin\theta_o}{\lambda}, \qquad \theta_o = -\theta_i. \tag{7}$$

The corresponding relevant roughness, σ_{rel}, is given by the square root of the volume under the relevant portion of the surface PSD illustrated in Fig. 3(b). It is thus calculated by the following integral:[33]

$$\sigma_{\mathrm{rel}}(\lambda,\theta_i) = \sqrt{\int_{-1/\lambda+f_o}^{1/\lambda+f_o} \int_{-\sqrt{1/\lambda^2-(f_x-f_o)^2}}^{\sqrt{1/\lambda^2-(f_x-f_o)^2}} \mathrm{PSD}(f_x,f_y)\,\mathrm{d}f_x\mathrm{d}f_y}. \tag{8}$$

It is the relevant roughness, σ_{rel}, that determines the fraction of the total reflected light contained in the specular beam and in the associated scattering function. For normal incidence (and isotropic roughness), the relevant roughness expressed by Eq. (8) simplifies to

$$\sigma_{\mathrm{rel}}(\lambda) = \sqrt{2\pi \int_{f=0}^{1/\lambda} \mathrm{PSD}(f)\,f\,\mathrm{d}f}. \tag{9}$$

For some applications, there is a nonzero low spatial frequency band limit, $1/L$, where L represents an inherent measurement bandwidth limit.[17,19,34,35] For example, if surface roughness is being inferred from TIS measurements, the upper and lower angle limits of the TIS instrument determine (through the grating equation) the minimum and maximum spatial frequency band limits of the resulting predicted surface roughness. Thus TIS measurements are meaningful only when the limiting angles are known and reported. The

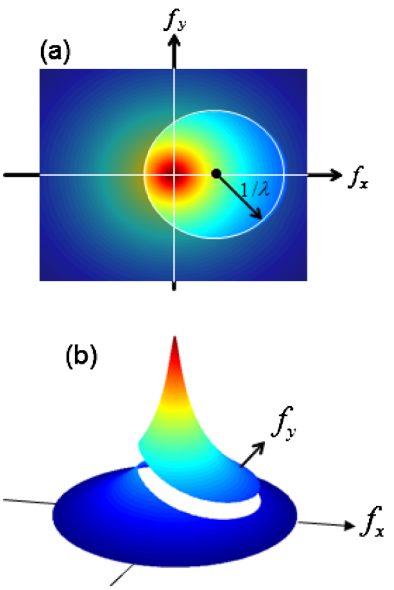

Fig. 3 (a) Illustration of the $2-D$ boundary of the appropriate band-limited portion of the surface PSD for an arbitrary incident angle, θ_i. (b) Illustration of the relevant portion of the surface PSD, whose integral yields the square of the relevant rms surface roughness.

additional contribution to roughness due to spatial frequencies between zero and $1/L$ can often be ignored.

For a surface with a Gaussian ACV function

$$\mathrm{ACV}(r) = \sigma_{\mathrm{total}}^2 \exp[-(\sigma_{\mathrm{total}}^2/\ell^2)], \tag{10}$$

the surface PSD is also a Gaussian function:

$$\mathrm{PSD}(f) = \pi\ell^2\sigma_{\mathrm{total}}^2 \exp[-(\pi\ell f)^2]. \tag{11}$$

It can also be readily shown that the cumulative radial integral of a $2-D$ rotationally symmetric Gaussian function is proportional to one minus that Gaussian, and the proportionality constant is the total volume of the Gaussian function. Thus, integrating Eq. (11) we obtain

$$\int_{\phi=0}^{2\pi}\int_{f=0}^{f} \mathrm{PSD}(f) f \mathrm{d}f\mathrm{d}\phi = \sigma_{\mathrm{total}}^2[1-\exp(-(\pi\ell f)^2)]. \tag{12}$$

But if the upper limit is set to $1/\lambda$, the integral on the left-hand side of Eq. (12) is just the bandlimited surface variance, σ_{rel}^2, for normal incidence. We thus have

$$\frac{\sigma_{\mathrm{rel}}^2}{\sigma_{\mathrm{total}}^2} = 1-\exp[-(\pi\ell/\lambda)^2]. \tag{13}$$

Figure 4 shows a family of parametric curves illustrating the ratio of σ_{rel}^2 to $\sigma_{\mathrm{total}}^2$ for different incident angles as a function of normalized correlation width. These curves were obtained by numerically integrating the relevant portion of the surface PSD as indicated in Eq. (8). The analytic solution for normal incidence is also included as a check on our numerical model.

However, optical surfaces fabricated by conventional grinding and polishing techniques on ordinary amorphous glassy materials and thin film coatings seldom exhibit Gaussian surface ACV functions. Church[36,37] has reported upon the fractal nature of many surface finishes, thus suggesting that the surface PSD can be modeled as exhibiting an inverse power law behavior at high spatial frequencies that can conveniently be fit by the following *ABC*, or *K* correlation, function of the form

$$\mathrm{PSD}(f)_{1-D} = \frac{A}{[1+(Bf)^2]^{C/2}}. \tag{14}$$

Here A is the height of the low spatial frequency plateau of the $1-D$ surface PSD and $1/B$ is the location of the knee in the log–log plot of the $1-D$ PSD (B can be considered the correlation width of the surface irregularities).

It has also been demonstrated that thin film coatings exhibit *ABC* (or combinations of *ABC*) PSD's describing the substrate and the intrinsic roughness of the coating.[30,38]

Assuming isotropic roughness, this $1-D$ measured surface PSD can be converted into the following $2-D$ surface PSD that relates more directly to the surface scatter behavior and hence to the resulting image degradation:

$$\mathrm{PSD}(f)_{2-D} = K\frac{AB}{[1+(Bf)^2]^{(C+1)/2}}, \qquad K = \frac{1}{2\sqrt{\pi}}\frac{\Gamma((C+1)/2)}{\Gamma(C/2)} \tag{15}$$

There is also a convenient analytic expression for the total volume under the $2-D$ surface PSD:

$$\sigma_{\mathrm{total}}^2 = \frac{2\pi KAB}{[(C-1)B^2]}, \tag{16}$$

and even an analytic expression for the $2-D$ Fourier transform of the above $2-D$ surface PSD. This surface ACV function is given by

$$\mathrm{ACV}(r) = (2\pi)^{1/2}\frac{A}{B}\frac{2^{-C/2}}{\Gamma(C/2)}\left(\frac{2\pi r}{B}\right)^{(C-1)/2}\mathcal{K}_{(C-1)/2}\left(\frac{2\pi r}{B}\right). \tag{17}$$

Although surface scatter effects can also be important at visible and infrared wavelengths, we will consider an ultraviolet example with a wavelength of 100 nm at normal incidence to a surface with a PSD given by Eq. (15). Figure 5 illustrates the ratio of σ_{rel}^2 to $\sigma_{\mathrm{total}}^2$ as a function of the surface correlation width B for several different values of the parameter C when the parameter $A = 6.10\ \mathrm{nm}^2\,\mathrm{mm}$. As

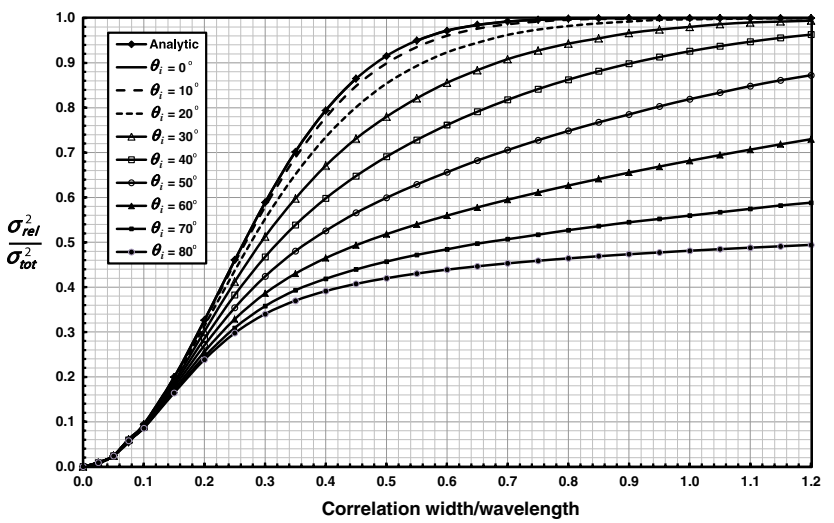

Fig. 4 Parametric curves illustrating the variation of relevant roughness with incident angle and surface correlation width (Gaussian ACV function).

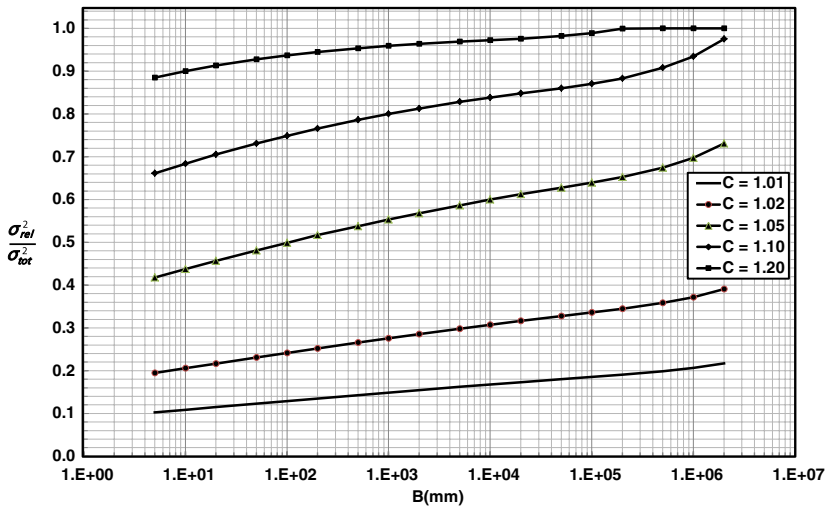

Fig. 5 Parametric curves illustrating the variation of relevant roughness with the parameters *B* and *C*.

for the case of the Gaussian PSD, the relevant roughness decreases with decreasing surface correlation width. And, of course, the relevant roughness increases with increasing C as a larger portion of the total roughness is contained within the circular bandlimited boundary for an inverse power law with a steeper slope. Note that a small percent change in the parameter C caused a greater change in the ratio of σ^2_{rel} to σ^2_{total} than did five decades of variation in the parameter B.

To provide even more insight into the nature of band-limited roughness for practical optical surfaces, Fig. 6 illustrates the ratio of σ^2_{rel} to σ^2_{total} as a function of the parameter C for fixed values of A and B ($A = 6.10$ nm^2 mm and $B = 120$ mm), but for different incident angles and wavelengths. Recall that the total surface variance, σ^2_{total}, is infinite for $C < 1.0$ (an inverse power law slope with a magnitude less than 2). The band-limited surface variance, σ^2_{rel}, thus initially increases rapidly from $C = 0$, then asymptotically approaches σ^2_{total} for $C > 1.35$ for an EUV wavelength of 30 nm. Increasing the wavelength by a factor of 333 to 10 μm only moves this asymptotic behavior out to a C-value of $\sim$1.75. It is thus apparent from Fig. 6 that the ratio of σ^2_{rel} to σ^2_{total} is quite insensitive to both incident angle and wavelength for surfaces with an *ABC* function PSD.

3 Total Integrated Scatter

Note that the surface correlation width does not appear explicitly in Eq. (5) or Eq. (6) for TIS. Yet Elson[7] was aware in 1983 that the derivation of Eq. (4) involved an assumption that the correlation width was long compared with the wavelength ($\ell \gg \lambda$). He also recognized that any surface spatial wavelengths shorter than the wavelength of the incident radiation would not contribute to the normal incidence TIS. Equation (4) is thus not valid in general, even for smooth surfaces. He then calculated that for $\ell \ll \lambda$, the value of TIS varies inversely as the fourth power of the wavelength for a smooth surface with a Gaussian ACV function illuminated at normal incidence,[7] so that TIS is

$$TIS = \left(\frac{64}{3}\right)\left(\frac{\pi^4\sigma^2\ell^2}{\lambda^4}\right), \qquad \ell \ll \lambda. \tag{18}$$

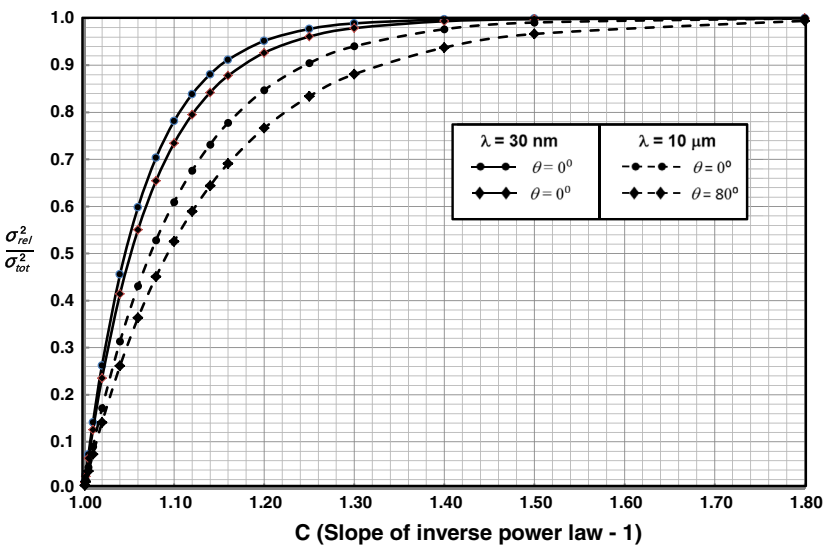

Fig. 6 Variation of relevant roughness to parameter *C*. Note insensitivity to incident angle.

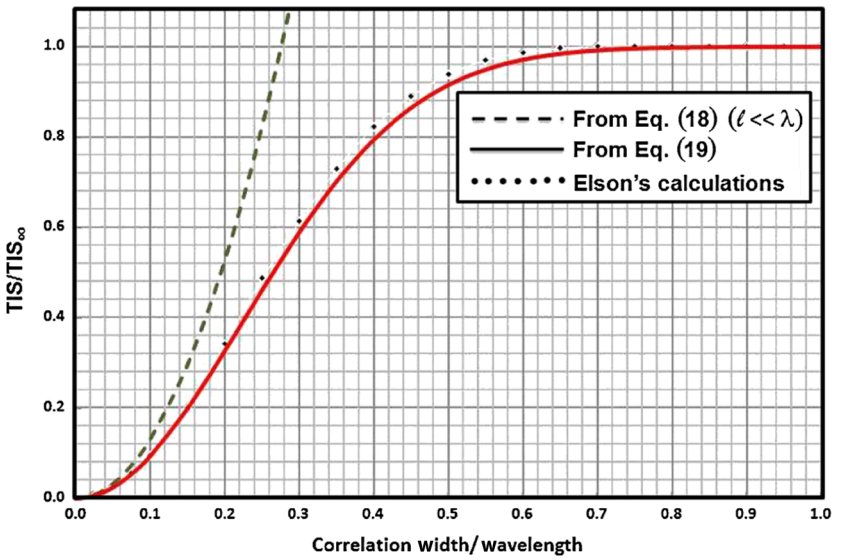

Fig. 7 TIS/TIS_∞ versus ℓ/λ for a smooth surface with normally incident light. The solid line is in excellent agreement with Elson's original analysis.

Elson continued his analysis of the variation of TIS with correlation width by plotting the ratio of the actual TIS for arbitrary correlation widths to TIS_∞, which is given by Eq. (4) when $\ell \gg \lambda$. He calculated the actual TIS by performing numerical integrations of the ARS predicted by the Rayleigh-Rice surface scatter theory. The result of these calculations is illustrated by the discrete data points in Fig. 7. Elson's quantity TIS/TIS_∞ (plotted as the solid line in Fig. 7) can also be calculated by merely dividing Eq. (5) by Eq. (3):

$$\frac{TIS}{TIS_\infty} = \frac{1 - \exp[-(4\pi \cos\theta_i \sigma_{\text{rel}}/\lambda)^2]}{1 - \exp[-(4\pi \cos\theta_i \sigma_{\text{total}}/\lambda)^2]}. \tag{19}$$

Both the numerator and the denominator of this ratio are equal for large correlation widths, yielding a value of unity for the ratio. There are thus two asymptotic regions in Fig. 7 with analytic solutions, illustrated by the dashed line given by Eq. (18) for $\ell \ll \lambda$, and unity as ℓ approaches λ. Equation (18) for small correlation widths has been quite useful in predicting surface scatter from optical thin films exhibiting columnar growth.[39,40]

Elson performed the above analysis, which provides valuable insight into surface scatter behavior, without ever mentioning or acknowledging the concept of band-limited roughness. He also determined that Eq. (4) is not limited to surfaces with a Gaussian surface height distribution function or a Gaussian ACV function.[7,19]

The excellent agreement between Elson's calculations and the predictions from Eq. (19) dramatically illustrates that Eqs. (3) and (4) are ambiguous and incorrect for surfaces with correlation widths less than the wavelength of the operational wavelength due to their failure to identify the relevant spatial frequency bandwidth limits, as does Eq. (5). Furthermore, by merely performing the $2 - D$ integral of the surface PSD over the shifted circular boundary discussed in section 2, we can readily calculate σ_{rel}, and therefore TIS, for arbitrary surface ACV functions without the necessity of implementing a given surface scatter theory to predict the ARS or the BRDF.

Since Eq. (19) is valid for surfaces with arbitrary roughness, correlation widths, and incident angles, a more thorough parametric analysis, providing even more insight into surface scatter phenomena, can now be readily performed. Figure 8 illustrates a set of parametric curves of TIS/TIS_∞ versus correlation width for different surface roughnesses ($0.02 < \sigma/\lambda < 0.50$) for a surface with a Gaussian ACV function. Again, the smooth surface curve agrees very well with Elson's original data.

Figure 9 illustrates a similar set of parametric curves of TIS/TIS_∞ versus incident angle for a fixed correlation width of $\ell/\lambda = 1.0$. This is again for surfaces exhibiting a Gaussian ACV function. Note that TIS/TIS_∞ is equal to unity, as expected for small incident angles. At an incident angle of about 30 deg, the curves diverge until about 65 deg. They then asymptotically converge to a common value of 0.455 at grazing incidence.

This behavior becomes intuitive when one realizes that even moderately rough surfaces become specular at grazing incidence. Both the numerator and the denominator thus become zero, and Eq. (19) becomes indeterminant for $\theta_i = 90$ deg. Applying L'Hospital's Rule yields TIS/TIS_∞ equal to

$$\frac{TIS}{TIS_\infty} = \frac{1 - \exp[-(4\pi \cos\theta_i \sigma_{\text{rel}}/\lambda)^2]}{1 - \exp[-(4\pi \cos\theta_i \sigma_{\text{total}}/\lambda)^2]} \rightarrow \frac{\sigma_{\text{rel}}^2}{\sigma_{\text{total}}^2} \quad \text{as } \theta_i \rightarrow 90^\circ \tag{20}$$

for all roughness values. Clearly, this asymptotic value of TIS/TIS_∞ will vary for different correlation widths. For example, for a correlation width of 2.0λ, we obtain the set of parametric curves illustrated in Fig. 10. For this case, the values of TIS/TIS_∞ are drastically different at normal incidence for different roughnesses, having substantially lower values for the smoother surfaces. And, indeed, the asymptotic value for grazing incidence has been reduced to a value of 0.236.

Figure 11 illustrates cumulative surface roughness as a function of spatial frequency for a state-of-the-art EUV telescope mirror characterized by an *ABC* function PSD.[41]

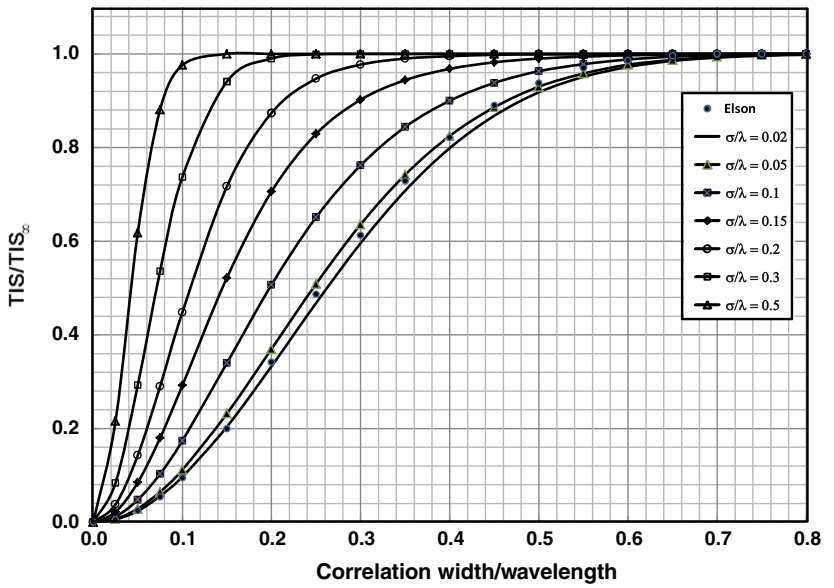

Fig. 8 Parametric curves of TIS/TIS$_\infty$ versus ℓ/λ for surfaces with a Gaussian ACV and different roughnesses for normally incident light.

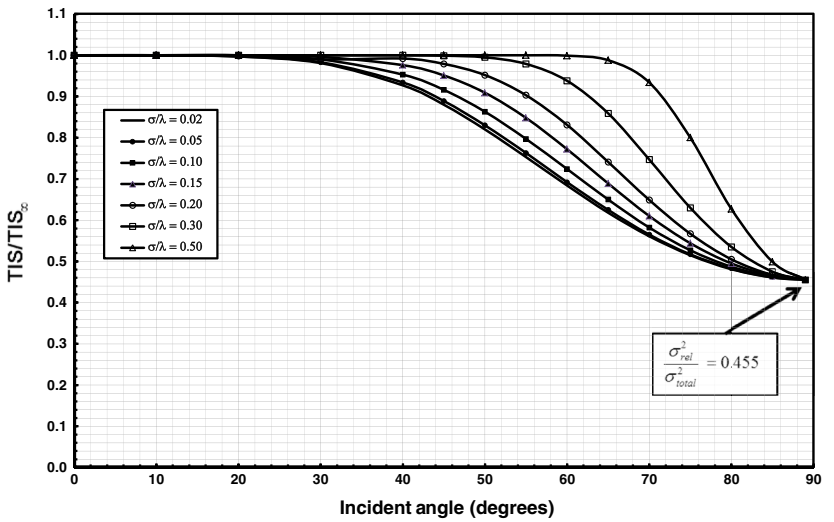

Fig. 9 Parametric curves of TIS/TIS$_\infty$ versus incident angle for surfaces of different roughnesses with a Gaussian ACV and $\ell/\lambda = 1.0$.

The relevant roughness (determined by a wavelength of 303.8 Å) is indicated, as is the total intrinsic roughness. The values of the *ABC* parameters are indicated in the figure, and several different metrology regions are shown over which band-limited optical fabrication tolerances are specified. The maximum relevant spatial frequency, relevant surface roughness, and resulting TIS as calculated from Eq. (5) are tabulated for each of six specific EUV wavelengths of interest. Note that at the longest wavelength of interest, only 7% of the reflected radiant power is scattered, whereas for the shortest wavelength of interest, over 56% of the reflected radiant power is scattered.

4 Predicting BRDF's for Arbitrary Roughness, Correlation Widths, and Incident Angles

The TIS of an optical surface can be a very useful metric for evaluating different optical materials and optical fabrication processes, particularly for short-wavelength imaging systems. However, when making image quality predictions from optical metrology data, or when deriving practical optical fabrication tolerances necessary to satisfy specific image quality requirements, it is frequently not sufficient to merely know the TIS. It is often necessary to also know the angular distribution of the scattered radiation, i.e., the ARS or the BRDF for different incident angles and wavelengths. Rayleigh-Rice,[42,6] Beckmann–Kirchhoff,[43] or Harvey–Shack[44,45] surface scatter theory is commonly used to predict surface scatter effects.

For short-wavelength imaging systems, where even state-of-the-art surfaces are moderately rough, this is a complicated problem that requires more than knowledge of the relevant bandlimited roughness of the optical surfaces making up the imaging system. The smooth-surface limitation of the classical Rayleigh–Rice surface scatter theory and the

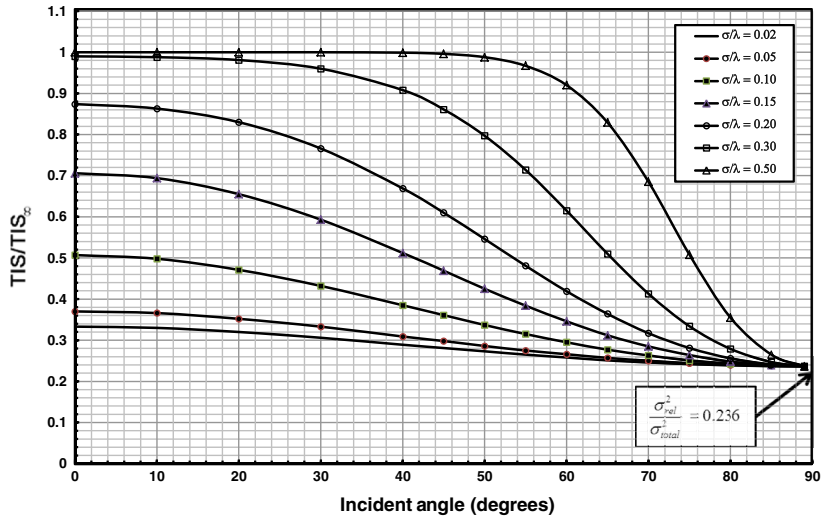

Fig. 10 Parametric curves of TIS/TIS$_\infty$ versus incident angle for surfaces of different roughnesses with a Gaussian ACV and $\ell/\lambda = 2.0$.

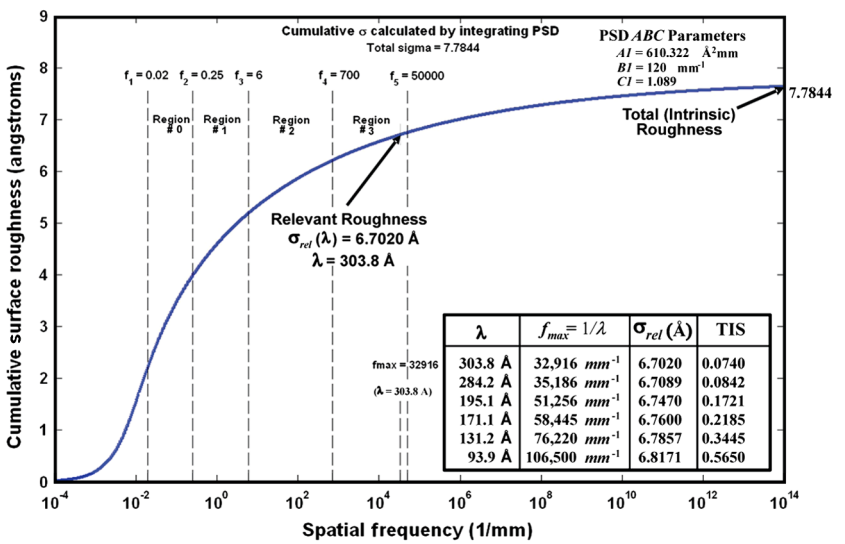

Fig. 11 Plot of cumulative surface roughness versus spatial frequency illustrates the difference between the relative roughness and the total roughness of an EUV telescope mirror characterized by an *ABC* function surface PSD. The TIS is tabulated for each of six EUV wavelengths of interest.

paraxial limitation of the Beckmann–Kirchhoff and the original Harvey–Shack theories have inhibited the widespread analysis of image degradation due to surface scatter phenomena. However, recent advances in surface scatter theory have resulted in a unified theory[46–48] that appears to combine the advantages of the Rayleigh–Rice theory and the Beckmann–Kirchhoff theories without the disadvantages of either. This generalized Harvey–Shack surface scatter theory has been demonstrated to be in good agreement with rigorous calculations and experimental results, even for moderately rough surfaces with arbitrary incident and scattered angles.[48]

As an example of the capabilities of the generalized Harvey-Shack surface scatter theory, Fig. 12 illustrates the previous TIS curves from Fig. 8 with a variety of inserts depicting the ARS curves corresponding to specific surface roughness and correlation width values. The ARS curves are all plotted on the same scale so one can readily see that the peak scattered intensity is (i) small in insert 1 due to the low TIS for this smooth surface, (ii) large in insert 3 due to the large TIS and correlation width, and (iii) small in insert 6 due to the small correlation width that causes σ^2_{rel} to be a small fraction of σ^2_{total}, thus reducing the TIS in spite of the fact that the surface is quite rough. Additional insight can be gained by studying the values of TIS, the ratio of σ^2_{rel} to σ^2_{total}, and TIS/TIS$_\infty$ for each of the six points represented by the ARS inserts. Table 1 provides these tabulated data.

The ARS data represented by the inserts in Fig. 12 can be input into several commercially available image analysis codes for predicting image quality as degraded by not only diffraction effects and geometrical aberrations, but surface scatter effects resulting from residual optical fabrication errors.[49] Finally, it should again be mentioned that many deep ultraviolet and EUV components involve multilayer coatings that require multilayer scattering theories, or scatter measurements at the operational wavelength.[29–32]

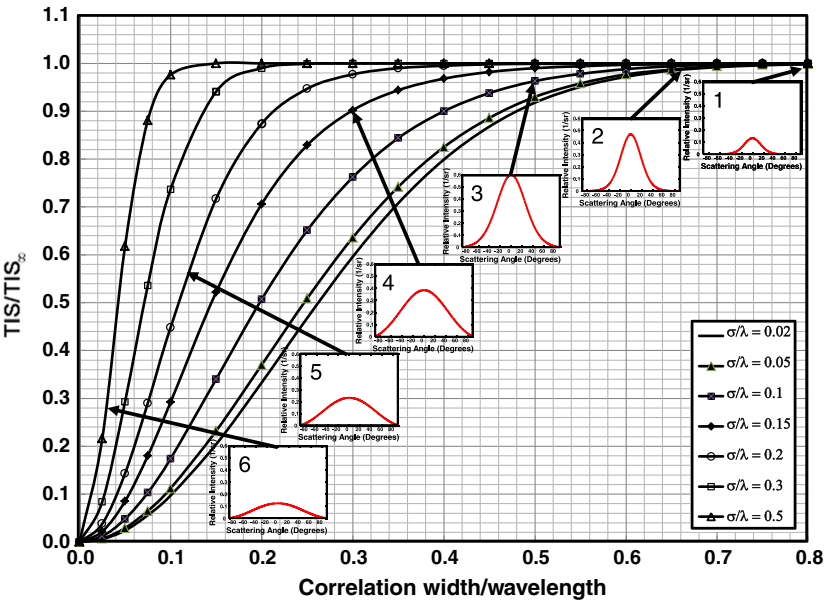

Fig. 12 Inserts added to Fig. 8 depict ARS curves calculated with the generalized Harvey-Shack surface scatter theory, which has been demonstrated to be valid for moderately rough surfaces with arbitrary correlation widths and incident angles.

Table 1 Tabulated data for each point represented by ARS inserts.

	σ/λ	ℓ/λ	TIS	$\sigma^2_{rel}/\sigma^2_{total}$	TIS/TIS_∞
1	0.02	0.80	0.0611	0.9980	0.9981
2	0.05	0.66	0.3225	0.9861	0.9886
3	0.10	0.50	0.7642	0.9150	0.9627
4	0.15	0.30	0.8765	0.5886	0.9023
5	0.20	0.12	0.5668	0.1325	0.5679
6	0.50	0.03	0.2945	0.0088	0.2945

5 Summary and Conclusions

We first reviewed the historical (50-year-old) expression for TIS as a function of rms surface roughness, and its widely used smooth surface approximation. This was followed by a thorough discussion of the spatial frequency bandlimited roughness of an optical surface that is *relevant* to surface scatter phenomena. A simple procedure for calculating that relevant roughness for arbitrary surface PSDs, wavelengths, and incident angles was presented.

The classical equation for calculating TIS was then updated to be explicitly expressed in terms of this relevant band-limited roughness. Only then does it properly account for the effects upon the TIS caused by variations in surface correlation width, wavelength, and incident angle. The resulting Eq. (5) incorporates the concept of the relevant bandlimited roughness into the definition of TIS and renders the classical ambiguous expressions for TIS, Eqs. (3) and (4), obsolete and inaccurate for many applications involving short surface correlation widths and large incident angles.

Extensive parametric predictions were then presented of the TIS for optical surfaces of arbitrary roughness, correlation widths, and incident angles. This parametric analysis provides valuable insight and understanding to optical fabrication and metrology engineers that is not readily available from the previously existing literature.

Finally, the capabilities of a new unified surface scatter theory combining the advantages of both the classical Rayleigh-Rice and Beckmann-Kirchhoff theories was demonstrated by calculating ARS curves for surfaces with arbitrary roughness, correlation widths, and incident angles.

We have not proven, either by experimental verification or by rigorous numerical electromagnetic theory, that Eq. (5) is accurate for roughnesses and incident angles that result in arbitrarily high TIS values; however, there have been numerical validations by the optical design community[50] that the complementary expression for the fraction of the energy remaining in the image core (when degraded by a combination of various aberrations, or figure errors, rather than microroughness) is accurate for values of Strehl ≥ 0.1. This would correspond to TIS ≤ 0.9. It is the authors' hope that the publication of this paper will not only benefit metrology engineers and image analysts, but also stimulate the more theoretically inclined readers to help determine the limit of the validity of Eq. (5).

References

1. H. E. Bennett and J. O. Porteus, "Relation between surface roughness and specular reflectance at normal incidence," *J. Opt. Soc. Am.* **51**(2), 123–129 (1961).
2. H. Davies, "The reflection of electromagnetic waves from a rough surface," *Proc. IEE. Pt. III* **101**(7), 209–214 (1954).
3. H. E. Bennett, "Specular reflectance of aluminized ground glass and the height distribution of surface irregularities," *J. Opt. Soc. Am.* **53**(12), 1389–1394 (1963).
4. V. Rehn et al., "Total integrated optical scattering in the vacuum ultraviolet," *Appl. Opt.* **16**(5), 1111–1112 (1977).
5. H. E. Bennett, "Scattering characteristics of optical materials," *Opt. Eng.* **17**(5), 480–488 (1978).
6. E. L. Church, H. A. Jenkinson, and J. M. Zavada, "Relationship between surface scattering and microtopographic features," *Opt. Eng.* **18**(2), 125–136 (1979).

7. J. M. Elson, J. P. Rahn, and J. M. Bennett, "Relationship of the total integrated scattering from multilayer-coated optics to angle of incidence, polarization, correlation length, and roughness cross-correlation properties," *Appl. Opt.* **22**(20), 3207–3219 (15 October 1983).
8. J. C. Stover, S. A. Serati, and C. H. Gillespie, "Calculation of surface statistics from light scatter," *Opt. Eng.* **23**(4), 406–412 (1984).
9. J. M. Bennett and L. Mattsson, *Introduction to Surface Roughness and Scattering*, Optical Society of America, Washington, DC (1989).
10. O. Kienzle, J. Staub, and T. Tschudi, "Light scattering from transparent substrates: theory and experiment," *Phys. Rev. B* **50**(3), 1848–1860 (15 July 1994).
11. T. Lindstrom and D. Ronnow, "Total integrated scattering from transparent substrates in the infrared region: validity of scalar theory," *Opt. Eng.* **39**(2), 478–487 (February 2000).
12. J. B. Hadaway et al., "Real-time total integrated scattering measurements on the Mir spacecraft to evaluate sample degradation in space," *Appl. Opt.* **40**(16), 2755–2768 (1 June 2001).
13. Breault Research Organization, *ASAP Tutorial: Stray Light Analysis with ASAP*, Tucson, AR (2008).
14. Semiconductor Equipment and Materials International, "Test method for measuring reflective total integrated scatter (TIS)," SEMI Standard MF1048-1111, www.semi.org.
15. International Organization for Standardization, *Optics and Optical Instruments—Test Methods for Radiation Scattered by Optical Components*, ISO, p. 13696 (2002).
16. E. L. Church, "Role of surface topography in x-ray scattering," *Proc. SPIE 184, Space Optics–Imaging X-ray Optics Workshop*, pp. 196–202 (1979).
17. E. L. Church and P. Z. Takacs, "Instrumental effects in surface finish measurements," *Proc. SPIE* **1009**, 46–55 (1988).
18. E. L. Church and P. Z. Takacs, "Light scattering from non-Gaussian surfaces," *Proc. SPIE* **2541**, 91–107 (1995).
19. J. C. Stover, *Optical Scattering, Measurement and Analysis*, 2nd ed., SPIE Optical Engineering Press, Bellingham, WA (1995).
20. T. A. Germer and C. C. Asmail, "Proposed methodology for characterization of microroughnessinduced optical scatter instrumentation," *Proc. SPIE* **2862**, 12–17 (1996).
21. M. G. Dittman, "No such thing as σ: flowdown and measurement of surface roughness requirements," *Proc. SPIE* **6291**, 1–8 (2006).
22. M. G. Dittman, "*K*-correlation power spectral density and surface scatter model," *Proc. SPIE* **6291**, 1–12 (2006).
23. D. Aikens, "Specification and control of mid-spatial frequency wavefront errors in optical systems," presented at the *Optical Society of America Topical Technical Digest Meeting on Optical Fabrication and Testing*, Rochester, NY, Paper OTuA1 (2008).
24. P. Murphy, "Methods and challenges in quantifying mid-spatial frequencies," presented at the *OSA Technical Digest Topical Meeting on Optical Fabrication and Testing*, Rochester, NY, Paper OTuA3 (2008).
25. A. Duparré, "Characterization of surface and thin-film roughness using PSD functions," presented at the *OSA Topical Meeting on Optical Fabrication and Testing*, Rochester, NY (2008).
26. R. J. Noll, "Effect of mid and high spatial frequencies on optical performance," *Opt. Eng.* **18**(2), 137–142 (1979).
27. J. E. Harvey and A. Kotha, "Scattering effects from residual optical fabrication errors," *Proc. SPIE* **2576**, 155–174 (1995).
28. J. E. Harvey, "Bridging the gap between 'figure' and 'finish'," presented at the *OSA Optical Fabrication and Testing Meeting*, Boston, MA (May 3 1996).
29. S. Schröder, S. Gliech, and A. Duparré, "Measurement system to determine the total and angle-resolved light scattering of optical components in the deep-ultraviolet and vacuum-ultraviolet spectral regions," *Appl. Opt.* **44**(29), 6093–6107 (October 2005).
30. S. Schröder et al., "Angle-resolved scattering and reflectance of extreme-ultraviolet multilayer coatings: measurement and analysis," *Appl. Opt.* **49**(9), 1503–1512 (20 March 2010).
31. S. Schröder et al., "Angle-resolved scattering: an effective method for characterizing thin-film coatings," *Appl. Opt.* **50**(9), C164–C171 (20 March 2011).
32. M. Trost et al., "Influence of the substrate finish and thin film roughness on the optical performance of Mo/Si multilayers," *Appl. Opt.* **50**(9), C148–C153 (20 March 2011).
33. J. E. Harvey et al., "Scattering from moderately rough interfaces between two arbitrary media," *Proc. SPIE* **7794** 77940V (2010).
34. E. L. Church and P. Z. Takacs, "Effects of the optical transfer function in surface profile measurements," *Proc. SPIE* **1164**, 46–59 (1989).
35. A. Duparré et al., "Surface characterization techniques for determining the root-mean-square roughness and power spectral densities of optical components," *Appl. Opt.* **41**(1), 154–171 (2002).
36. E. L. Church, "Fractal surface finish," *Appl. Opt.* **27**(8), 1518–1526 (15 April 1988).
37. E. L. Church, P. Z. Takacs, and T. A. Leonard, "The prediction of BRDFs from surface profile measurements," *Proc. SPIE* **1165**, 136–150 (1989).
38. J. Ferré-Borrull, A. Duparré, and E. Quesnel, "Procedure to characterize microroughness of optical thin films: application to ion-beam-sputtered vacuum-ultraviolet coatings," *Appl. Opt.* **40**(13), 2190–2199 (1 May 2001).
39. A. Duparré and S. Kassam, "Relation between light scattering and the microstructure of optical thin films," *Appl. Opt.* **32**(28), 5475–5480 (1993).
40. A. Duparré, "Scattering from surfaces and thin films," in *Encyclopedia of Modern Optics*, B. D. Guenther, D. G. Steel, and L. Bayvel, eds., Elsevier, Amsterdam (2004).
41. D. Martinez-Galarce et al., "A novel forward-model technique for estimating EUV imaging performance—design and analysis of the SUVI telescope," *Proc. SPIE* **7732**, 773237 (2010).
42. S. O. Rice, "Reflection of electromagnetic waves from slightly rough surfaces," *Commun. Pure Appl. Math.* **4**(2–3), 351–378 (1951).
43. P. Beckmann and A. Spizzichino, *The Scattering of Electromagnetic Waves from Rough Surfaces*, Pergamon Press, New York (1963).
44. J. E. Harvey, "Light-scattering characteristics of optical surfaces," Ph.D dissertation, University of Arizona (1976).
45. J. E. Harvey, "Surface scatter phenomena: a linear, shift-invariant process," in *Scatter from Optical Components*, J. C. Stover, ed., *Proc. SPIE* **1165**, 87–99 (1989).
46. J. E. Harvey, A. Krywonos, and J. C. Stover, "Unified scatter model for rough surfaces at large incident and scattered angles," SPIE International Symposium on Optics and Photonics, *Proc. SPIE* **6672**, 66720C (2007).
47. J. E. Harvey et al., "Calculating BRDFs from surface PSDs for moderately rough surfaces," *Proc. SPIE* **7426**, 74260I (2009).
48. A. Krywonos, J. E. Harvey, and N. Choi, "Linear systems formulation of surface scatter theory for rough surfaces with arbitrary incident and scattering angles," *J. Opt. Soc. Am. A* **28**(6), 1121–1138 (June 2011).
49. J. E. Harvey et al., "Image degradation due to scattering effects in two-mirror telescopes," *Opt. Eng.* **49**(6), 063202 (2010).
50. Zemax Development Corporation, *Zemax Optical Design Program User's Guide*, p. 182 (August 2007).

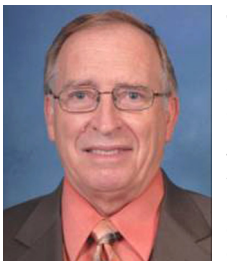

James E. Harvey is an associate professor in the College of Optics and Photonics at the University of Central Florida and a senior staff member of the Center for Research and Education in Optics and Lasers (CREOL). He has a PhD in optical sciences from the University of Arizona and is credited with over 195 publications and conference presentations in the areas of diffraction theory, surface scatter phenomena, adaptive optics, wavefront sensing, beam sampling technology, optical properties of materials, phased telescope arrays, and X-ray/EUV imaging systems. He is a member of OSA and a Fellow and past board member of SPIE.

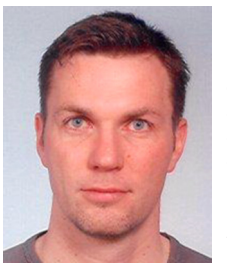

Sven Schroeder received his PhD degree in physics from the Friedrich Schiller University in Jena, Germany in 2008. His dissertation dealt with light scattering properties of optical surfaces and thin film coatings at 193 nm and 13.5 nm. He has been with the Surface and Thin Film Characterization group at the Fraunhofer Institute for Applied Optics and Precision Engineering (IOF) in Jena since 2004. In 2007, he was cowinner of the Thuringian Research Prize for IOF's contributions to the development of optical components and characterization techniques for EUV lithography. From July 2010 to July 2011 he was a visiting research scientist at CREOL/UCF in Orlando, Florida, working in the Imaging Group on light scattering models. He has 16 refereed journals to his credit.

Narak Choi received a bachelor's and a master's degree in physics from Seoul National University, South Korea, in 2005 and 2007, respectively. He is currently a PhD student at the College of Optics and Photonics at the University of Central Florida, doing research on surface scatter theory.

Angela Duparré received her PhD degree (thesis on optical properties of high-power laser mirrors) from the physics faculty of the Friedrich Schiller University of Jena in 1985. In 1992, she joined the Fraunhofer Institute for Applied Optics and Precision Engineering in Jena to become head of the Surface and Thin Film Characterization Group. Her interests have since been directed to the study of optical and non-optical surface and thin film properties such as light scattering, nano-/microstructures, and roughness, as well as to the development of light scattering measurement and modeling techniques. She has published more than 100 papers and is involved in standardization committees and in the organization of conferences on optical metrology, fabrication, and thin film coatings.